Original Article

Evaluation of Reconstruction Algorithms to Validate the NEMA Phantom Results in Clinical Scenario – A Comparative Study Using Time-of-Flight versus Non-Time-of-Flight Positron Emission Tomography Imaging

Ajay Kumar, Pearl Jacob, Ankit Watts, Anwin Joseph, Harneet Kaur, Monika Hooda, Amritjyot Kaur, Baljinder Singh

Department of Nuclear Medicine, Post Graduate Institute of Medical Education and Research, Chandigarh, India

Abstract

Objectives: The objective is to standardize the reconstruction parameters for the time-of-flight (TOF) *versus* non-TOF positron-emission tomography/computed tomography (PET/CT) imaging data and validation of the same in a clinical setting. **Methods:** The four spheres (10.0/13.0/17.0/22.0 mm) of the PET phantom (NEMA IQ Nu 2-2001) were filled with four times higher activity of [^{18}F]-NaF than the background (5.3kBq/mL). Imaging (image matrix – 128 × 128 × 47, 2 min, 3D model) was done using two different (TOF/non-TOF) PET scanners. Phantom data were reconstructed in TOF and non-TOF modes for lutetium–yttrium oxyorthosilicate and non-TOF mode for bismuth germanate-based PET scanners. The reconstructed data (by varying iteration and subsets) that provided the best image contrast and signal-to-noise ratio (SNR) were evaluated. The whole-body [^{18}F]-fludeoxyglucose (FDG) PET/CT scans (7–8 frames; 2.0 min/frame) in 16 lymphoma patients were acquired at 60 min after injecting the radioactivity (370.0–444.0 MBq of [^{18}F]-FDG. The clinical PET/CT data were reconstructed using phantom-derived reconstruction parameters and evaluated for image contrast and SNR of the detected lesions. **Results:** TOF reconstruction at second iteration provided significantly ($P \leq 0.02$) higher SNR (20.7) and contrast (contrast recovery coefficient/background variability = 3.21) for the smallest hot lesions (10.0 mm) in the phantom than the non-TOF system. Similarly, in patient data analysis for the selected FDG avid lesions, the SNR values were significantly ($P = 0.02$) higher (13.3 ± 6.49) in TOF than (11 ± 6.48) in non-TOF system. Further, the small (≤10.0 mm) lesions were seen more distinctly in TOF system. **Conclusion:** It is thus observed that TOF reconstruction converged faster than the non-TOF, and the applicability of the same may impact the image quality and interpretation in the clinical PET data. The validation of the phantom-based experimental reconstruction parameters to clinical PET imaging data is highly warranted.

Keywords: *Image contrast, NEMA IQ phantom, positron emission tomography Imaging, signal-to-noise ratio, time-of-flight/non-time-of-flight reconstruction*

Introduction

^{18}Fluorine-[^{18}F]-2-fluoro-2-deoxy-D-glucose positron emission tomography coupled with computed tomography ([^{18}F]-fludeoxyglucose [FDG] positron emission tomography/computed tomography [PET/CT]) has been recognized as a useful tool for the detection of various human malignancies.[1-5] A high image resolution and contrast are required for an accurate diagnosis and unequivocal interpretation of the whole-body reconstructed PET images. The information yielded by point-spread function and time-of-flight (TOF) concept has improved the spatial resolution and signal-to-noise ratio (SNR) and has provided high contrast PET images.[6,7]

Although the concept of using TOF was first proposed in the 1960's, it was limited due to the non-availabilty of fast and high-density detectors.[8,9] Later, an introduction of high-density bismuth germanate (BGO) detector provided high-sensitivity PET system but still was not suitable for use in TOF scanner. The technological advances in detector technology led to the development of lutetium oxyorthosilicate (LSO) and lutetium–yttrium oxyorthosilicate (LYSO) PET detectors which had ideal physical characteristics for TOF scheme.[10-12] The TOF concept estimates the difference in arrival times between a pair of coincident photons and increases the probability that

How to cite this article: Kumar A, Jacob P, Watts A, Joseph A, Kaur H, Hooda M, *et al.* Evaluation of reconstruction algorithms to validate the nema phantom results in clinical scenario – A comparative study using time-of-flight versus non-time-of-flight positron emission tomography imaging. Indian J Nucl Med 2022;37:113-20.

Address for correspondence:
Dr. Baljinder Singh, Department of Nuclear Medicine, Post Graduate Institute of Medical Education and Research, Chandigarh - 160 012, India. E-mail: drbsingh5144@yahoo.com

Received: 06-09-2021
Revised: 29-11-2021
Accepted: 30-11-2021
Published: 08-07-2022

Access this article online

Website: www.ijnm.in

DOI: 10.4103/ijnm.ijnm_137_21

Quick Response Code:

an annihilation event will be accurately located along the line of response. This additional information enables the reconstruction algorithm using a lesser number of iterations to converge to the expected image with a reduced noise level.[13] However, the performance of a TOF PET scanner in a given setting needs evaluation through the use of appropriate phantom/s for further clinical validation in patients' PET imaging data.

Recent studies have reported faster convergence of lesions' contrast and improvement in lesion/s detection with TOF.[6,13-17] In this study, we determined the optimal reconstruction parameters to enhance the effect of TOF on the image contrast and signal-to-noise ratio (SNR) using a PET-NEMA IQ phantom. The phantom-derived parameters were validated for the clinical imaging data sets acquired on TOF and non-TOF PET scanners.

Materials and Methods

Phantom study

Data acquisition and image reconstruction

The NEMA IQ NU 2-2001 phantom (Data Spectrum Corporation, Durham, USA) filled with [^{18}F]-sodium fluoride (NaF) was used for image acquisition on TOF-based Discovery PET/CT 710 scanner with LYSO crystal and non-TOF-based Discovery STE 16 with BGO crystal PET scanners (GE, Healthcare, Milwaukee, USA). The coincidence time and energy windows of TOF and non-TOF scanners were 4.9 ns and 12 ns and 425 keV–650 keV, respectively.

The four spheres (diameter 10.0, 13.0, 17.0, and 22.0-mm) of the phantom were filled with four times higher radioactivity of [^{18}F]-NaF than the background. The two largest spheres, 28.0 mm and 37.0 mm, were filled with water. The central lung insert was kept blank. The background was filled with activity concentration typical of what is used in a clinical [^{18}F] FDG-PET study (370 MBq/70-kg patient, or 5.3 kBq/mL).

The image acquisition was done in a 3D mode for 2 min and an image matrix of 128 × 128 × 47 and slice thickness of 3.3 mm were used for both scanners. For CT data acquisition (attenuation correction), voltage of 120 kV, current of 100 mA, tube rotation of 0.5 s, and slice collimation of 5.0 mm were used.

Reconstruction optimization

The acquired PET/CT phantom data were reconstructed using ordered-subset expectation maximization (OSEM) algorithm. The number of iterations was changed from 1 to 10 in reconstruction models, whereas the number of subsets was kept constant (12 for LYSO TOF and LYSO non-TOF and 14 for BGO non-TOF) for the two scanners. The post-smoothing filter of 6.0 mm was used in all reconstruction models. Lesion SNR, contrast, and noise were studied as a function of the iteration number for 10.0-, 13.0-, and 17.0-mm spheres.

Data analysis

The phantom PET images were analyzed by visual interpretation as well as by quantitative evaluation of SNR, contrast, and noise parameters for 10.0- and 13.0-mm hot spheres as a function of the iteration number.

For visual assessment, the PET images were evaluated for the detectability of 10.0-mm hot sphere using four-step scoring criteria (0– not visualized; 1– visualized but similar hot spots were observed elsewhere; 2– visualized but no similar hot spots were observed elsewhere; and 3-distinctly identifiable) by two experts which included a physicist and a nuclear medicine physician. These investigators were blinded to the location/slice number on which hot sphere was to be visualized.

A transverse slice in which the hot and cold spheres were visualized with the highest contrast was chosen. A circular region of intrest was placed around 10.0-, 13.0-, and 17.0-mm spheres well inside the lesion. A large circular ROI of 37.0 mm in diameter was drawn on the slice of the sphere center and on slices ±1 cm and ±2 cm away from the centered slice for calculating the background.

Signal-to-noise ratio

The lesion SNR was evaluated manually using the following mathematical formula:

$$\text{SNR} = \frac{\text{Signal}\left(\text{maximum value}\right) - \text{Background}\left(\text{mean value}\right)}{\text{SD}}$$

where signal is the maximum activity in the corresponding hot sphere ROI.

- The background is the mean of the maximum activity in the five background ROIs
- SD is the standard deviation in the five background values.

If the input contrast is known as *a priori*, then it is a measure of the convergence of an iterative algorithm.

$$\text{Contrast} = \frac{\text{Signal(maximum value)}}{\text{Background}\left(\text{mean value}\right)}$$

The noise, or normalized noise, is the undesired effect of convergence since the noise increases monotonically with each iteration. The noise was calculated as:

$$\text{Noise} = \frac{\text{SD}}{\text{Background}}$$

Contrast recovery coefficient and background variability

The percent contrast recovery coefficient ($CRC_{C,n}$) and percent background variability (BV_n) for each hot sphere "n" were calculated using the NEMA IQ analysis tool.

In this analysis, the computer software prompts for six spheres' ROIs, 1 ROI for lung and 12 ROIs for background in the central slice and in slices ±1 and ±2 cm away, thus using a total of 60 background ROIs.

$$CRC_{C,n} = 100 \times \frac{C_{B,n} - C_{C,n}}{C_{B,n}}$$

$$BV_n = 100 \times \frac{\sqrt{\frac{1}{K-1}\sum_{K=1}^{K}(C_{B,n,k} - C_{B,n})^2}}{C_{B,n}}$$

where $C_{B,n}$ is the average of the background ROI counts for sphere n, $C_{C,n}$ is average counts in the ROI for sphere n, and k is equal to the number of background ROIs.

Clinical study

We retrospectively evaluated the data of 16 (11 males: 5 females; mean age = 50.0 ± 17.5; range = 18–75 years) patients with confirmed diagnosis of lymphoma who were referred (between October 2014 and March 2015) to the Department of Nuclear Medicine for [^{18}F]-FDG PET/CT either for initial staging or for follow-up/response assessment. Out of 16, six patients had undergone scan on LYSO (PET) scanner and the remaining 10 patients in BGO non-TOF PET scanner.

Ethical considerations

The study did not involve any ethical issue as the design was mainly experimental work using [^{18}F]-NaF PET phantom imaging.[^{18}F]-FDG PET/CT data of patients who were referred routinely for the clinical indication was analyzed retrospectively. However, as a routine clinical practice, informed written consent was obtained from all the patients.

Data acquisition

PET/CT acquisition in 3D model was started at 60 min post intravenous (IV) injection of about 370.0–444.0 MBq activity of [^{18}F]-FDG in each patient. CT topogram was acquired to define the limits of the patients' scan acquisition. Thereafter, a whole-body CT scan was acquired with IV contrast with parameters of 120 kV, 350 mA, 0.5-s tube rotation, and 3.75-mm slice collimation. PET scan from the base of the skull to mid-thigh was acquired in 7–8 frames (2.0 min/frame).

Image reconstruction

The PET data acquired were reconstructed in both TOF and non-TOF modes on LYSO-based PET scanner and non-TOF mode based on BGO retrospectively using OSEM. Further, the data sets were reconstructed with two and three iterations with five subsets (12, 16, 18, 24, and 32) for TOF and non-TOF LYSO-based scanners and four subsets (14, 20, 28, and 35) for non-TOF BGO-based PET system.

Data analysis

The reconstructed PET data using the above mentioned iterations and subsets were analyzed using both qualitative and quantitative approaches. For quantitative analysis in each patient, the liver slice was considered background and the lesion was selected on the basis of the smallest identifiable lesion seen on MIP image for the particular iteration and subset and was extrapolated to all iterations and subsets using OSEM algorithm.

A visual scoring (qualitative) approach was used to define the image contrast on each slice, and the scoring was categorized and graded as below:

Qualitative visual interpretation

Lesion

1- defines lesions not able to differentiate; 2 – poorly differentiated; 3 – poorly differentiated along with hazy margin; 4 – lesions well delineated; and 5 – lesions differentiated distinctly

Background

1. No noise
2. Acceptable noise
3. Noisy
4. Very noisy (patchy Image)
5. Extremely noisy (noise equivalent to the usual small lesion)

The quantitative evaluation was performed by drawing a fixed ROI over the lesion to compute SUV_{max} and background as a mean of 10 measurements of SUV_{max} over the liver. In further analysis, the quantitative parameters of SNR, contrast, and noise were also evaluated as described above for phantom data analysis.

Statistical analysis

The statistical analysis was done using the SPSS Statistics-20 software. The paired *t*-test was used to test the differences in the manual and computer-based quantitative parameters such as SNR and CRC/BV between TOF and non-TOF reconstruction algorithms. A statistically significant difference was considered at $P \leq 0.05$.

Results

Phantom data

Qualitative analysis

On comparative visual analysis performed for phantom images reconstructed in TOF and non-TOF modes, it was found that the best image contrast was seen at iteration 2 for TOF and at iteration 3 for non-TOF systems, respectively [Table 1 and Figure 1].

Quantitative phantom image analysis

For the quantitative image analysis, two parameters, i.e., SNR and CRC/BV ratios, were evaluated for 10.0-mm

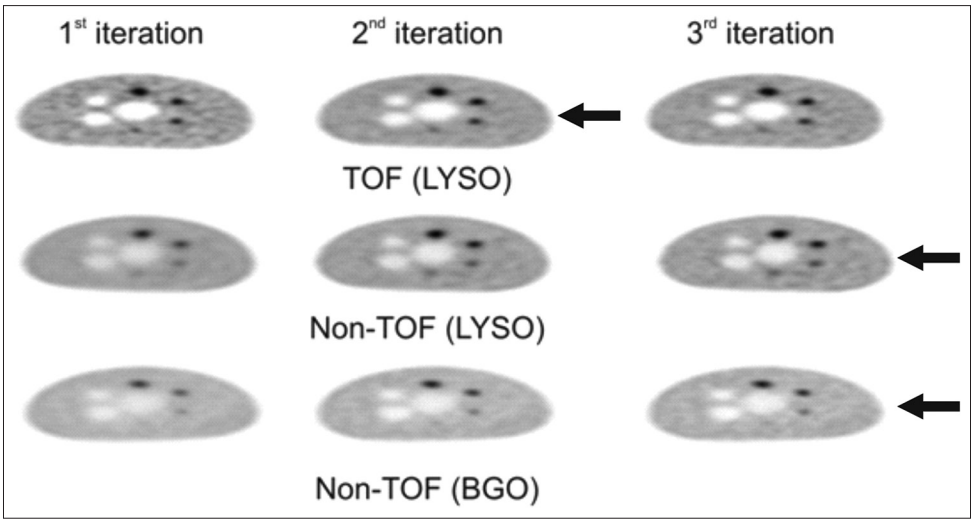

Figure 1: Transaxial images of NEMA NU-2 IQ phantom on visual analysis demonstrating best image contrast for 10.0-mm sphere (smallest sphere) at 2nd (Ist row), 3rd (2nd row), and 3rd (3rd row) iteration for lutetium–yttrium oxyorthosilicate time-of-flight, lutetium–yttrium oxyorthosilicate non-time-of-flight and bismuth germanate non-time-of-flight systems, respectively

Table 1: The visual scores of 10.0-mm lesion for various iterations of lutetium-yttrium oxyorthosilicate time-of-flight and (lutetium-yttrium oxyorthosilicate non-time-of-flight and bismuth germanate non-time-of-flight systems

Iteration number	LYSO PET system Visual score		BGO PET system Visual score
	TOF	non-ToF	non-TOF
1	2	0	0
2	3	1	1
3	2	3	2
4	2	2	1
5	2	1	1
6	2	1	1
7	2	1	1
8	2	1	1
9	1	1	1
10	1	1	1

PET: Positron-emission tomography, TOF: Time of flight, LYSO: Lutetium-yttrium oxyorthosilicate, BGO: Bismuth germanate

and 13.0-mm hot spheres, respectively. The results of this analysis are presented in Tables 2 and 3 and Figures 2 and 3.

Signal-to-noise ratio

The mean SNR values for 10.0-mm and 13.0-mm hot spheres were highest (20.66; 53.32) for TOF model at iteration 2 followed by LYSO non-TOF and BGO non-TOF at iteration 3 (10.80; 25.80) and 2 (8.5; 22.63), respectively [Table 2 and Figure 2]. It is highlighted that the SNR values (both for 10.0 and 13.0-mm spheres) for TOF were higher by a factor of 2.0 in comparison to the LYSO non-TOF and by a factor of about 2.5 times than the BGO non-TOF system. The SNR values for 10.0-mm hot sphere differed significantly ($P = 0.02$) between TOF and non-TOF systems; however, no significant difference ($P = 0.385$) was observed between the two non-TOF (LYSO/BGO) systems.

Contrast recovery coefficient/background variability ratios

The mean values of CRC/BV ratios were highest at iteration 2 both for 10.0-mm and 13.0-mm hot spheres (3.21; 6.5) for TOF system followed by LYSO non-TOF and BGO non-TOF systems at iteration 3 (2.34; 4.35) and at iteration 2 (1.58; 4.03), respectively [Table 3 and Figure 3]. It is pertinent to mention that the image contrast (CRC/BV) was about 1.5 times higher in TOF *versus* LYSO non-TOF. However, this ratio was higher by a factor of 2.0 times for 10.0-mm hot sphere in LYSO TOF *versus* BGO non-TOF PET system. The CRC/BV ratio for 10.0 mm hot sphere differed significantly ($P = 0.001$) between TOF and non-TOF systems; however, no significant difference was observed between the two non-TOF systems.

Patients positron-emission tomography/computed tomography data

Qualitative assessment

The visual analysis of the PET images of six patients reconstructed in LYSO TOF and LYSO non-TOF modes demonstrated that the best lesion/background ratio was seen at 2/12 [Figure 4a] and at 3/12 [Figure 4b] iteration/subset reconstruction algorithms for LYSO TOF and LYSO non-TOF systems, respectively. These findings in the patients' imaging data corroborated with the reconstruction parameters and image quality as observed for PET phantom data. Furthermore, a small lesion (<10.0 mm) was more distinctly identified in a patient in the TOF reconstructed image than that seen in non-TOF image [Figure 5].

Similarly, the visual analysis of the PET images of 10 patients reconstructed in BGO non-TOF depicted the highest lesion-to-background ratio at 2/14 iteration/subsets [Figure 4c]. These findings were in consonance with the results observed for phantom imaging data.

Table 2: The signal-to-noise ratio values obtained using lutetium-yttrium oxyorthosilicate (time-of-flight and non-time-of-flight) and bismuth germanate (non-time-of-flight) positron-emission tomography systems for 10-mm and 13-mm hot spheres at different iterations

Iterations	LYSO PET system SNR				BGO non-TOF SNR	
	10 mm		13 mm		10 mm	13 mm
	TOF	Non-TOF	TOF	Non-TOF	Non-TOF	Non-TOF
1	18.19	4.92	49.43	14.85	4.08	17.15
2	20.66	7.08	53.32	16.86	8.49	22.63
3	14.39	10.80	35.43	25.80	8.42	17.19
4	10.23	9.83	24.89	24.30	7.02	13.25
5	9.98	9.37	22.61	23.51	6.04	11.07
6	8.00	6.62	17.43	17.10	5.98	10.47
7	7.46	4.74	15.61	11.86	5.94	10.07
8	7.33	4.68	14.91	11.43	5.63	9.23
9	6.17	4.35	12.26	10.77	5.32	8.54
10	6.41	4.14	12.21	10.70	4.58	7.34

PET: Positron-emission tomography, TOF: Time of flight, LYSO: Lutetium-yttrium oxyorthosilicate, BGO: Bismuth germinate, SNR: Signal-to-noise ratio

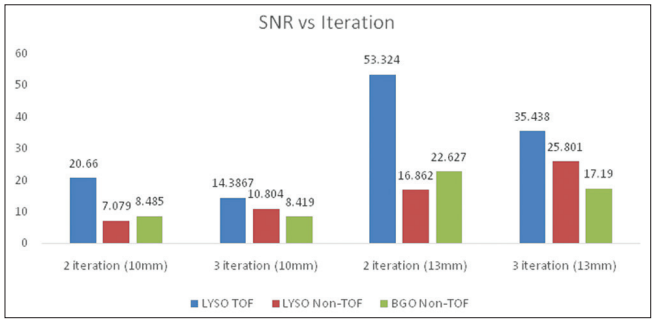

Figure 2: Bar diagram presenting signal -to-noise ratio values (Y-axis) for 10.0-mm and 13.0-mm hot spheres in lutetium–yttrium oxyorthosilicate time-of-flight lutetium–yttrium oxyorthosilicate non-time-of-flight and bismuth germanate non-time-of-flight systems at 2nd and 3rd iteration (X-axis), respectively

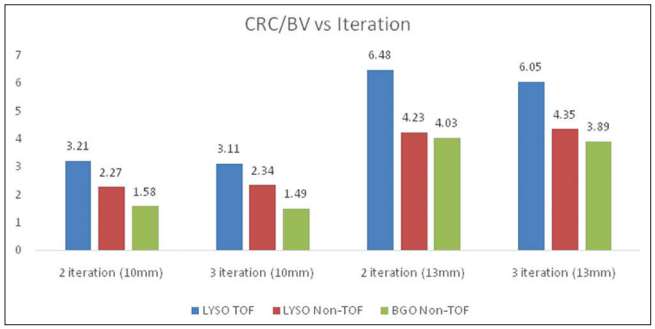

Figure 3: Bar diagram presenting contrast recovery coefficient/background variability values (Y-axis) for 10-mm and 13-mm hot spheres in lutetium–yttrium oxyorthosilicate time-of-flight, lutetium–yttrium oxyorthosilicate nontime-of-flight, and bismuth germanate nontime-of-flight systems at 2nd and 3rd iteration (X-axis), respectively

Quantitative assessment

The same lesions in six patients (one lesion/patient) which were used for visual analysis were also subjected to quantitative analysis to calculate the SNR using 2/12 and 3/12 (iteration/subset) in LYSO TOF and LYSO non-TOF, respectively. The SNR values were highest at 2/12 in TOF and at 3/12 in non-TOF reconstructive algorithms. The mean SNR value in TOF was (13.3 ± 6.49) significantly (P = 0.02) higher than that (11 ± 6.48) in non-TOF system [Table 4].

Similarly, the imaging data in 10 patients from BGO non-TOF system were also subjected to quantitative analysis to calculate the SNR ratio using 2/14 and 3/14 (iteration/subset) reconstruction algorithms. The results of this analysis revealed that the mean SNR value was (19.93 ± 16.60) significantly (P = 0.02) higher at 2/14 than (14.70 ± 13.16) at 3/14 reconstruction algorithms [Table 5].

Discussion

Advances in PET/CT technologies with the incorporation of TOF-LYSO concept have improved the detection of small lesions.[18] The detection limit using a conventional PET/CT is usually 1.0 cm, and the PET image quality is usually evaluated using a phantom with 10.0-mm (and above) hot spheres.[19] This validation is quintessential when the new PET/CT is being put to clinical use so as to ensure that the derived reconstruction parameters match with the vendor's provided parameters and thus can be used with confidence for the accurate performance of the system and interpretation of clinical PET imaging data prospectively.

The SNR values (both for 10.0- and 13.0-mm spheres) for LYSO TOF were higher by 2.0 fold in comparison with the LYSO non-TOF and by a factor of about 2.5 times than the BGO non-TOF system. The CRC/BV ratio was about 1.5 times higher for TOF *versus* LYSO non-TOF, whereas the ratio of LYSO TOF versus BGO non-TOF (for 10-mm-hot sphere) was higher by a factor of 2.0. The results obtained were concordant with those shown by Surti

Table 3: The contrast recovery coefficient/background variability ratios obtained in lutetium-yttrium oxyorthosilicate (time-of-flight and non-time-of-flight) and bismuth germanate (non-time-of-flight) positron-emission tomography systems of 10-mm and 13-mm hot spheres at different iterations

Iterations	LYSO PET system CRC/BV ratio				BGO non-TOF CRC/BV ratio	
	10 mm		13 mm		10 mm	13 mm
	TOF	Non-TOF	TOF	Non-TOF	Non-TOF	Non-TOF
1	2.66	1.67	5.44	3.88	0.666	3.17
2	3.21	2.27	6.48	4.23	1.58	4.03
3	3.11	2.34	6.05	4.35	1.49	3.89
4	2.82	2.31	5.23	4.33	1.49	3.896
5	2.86	2.30	5.38	4.25	1.49	3.35
6	2.56	2.24	5.05	4.13	1.49	3.93
7	2.52	2.17	4.82	3.98	1.40	3.33
8	2.44	2.12	4.7	3.87	1.32	3.07
9	2.42	2.09	4.61	3.75	1.36	3.45
10	2.33	2.06	4.46	3.65	1.22	2.64

PET: Positron-emission tomography, TOF: Time of flight, LYSO: Lutetium-yttrium oxyorthosilicate, BGO: Bismuth germinate, CRC/BV: Contrast recovery coefficient/background variability

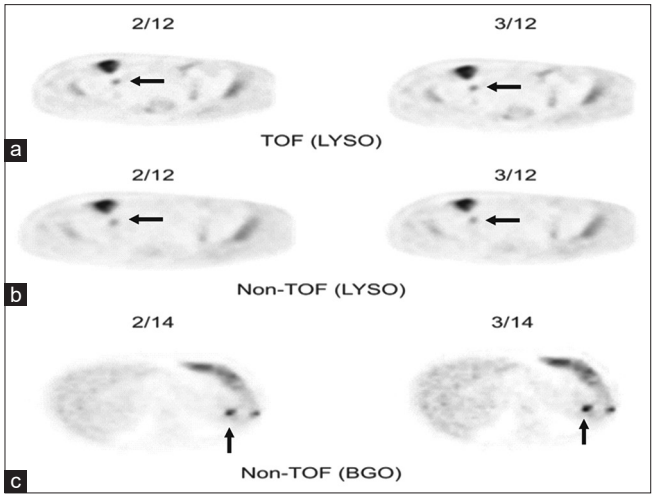

Figure 4: The visual image analysis in an 18-year-old NHL patient showing better lesion (right inguinal lymph node) contrast at 2/12 iteration (a) in lutetium–yttrium oxyorthosilicate time-of-flight positron-emission tomography and at 3/12 iteration (b) in lutetium–yttrium oxyorthosilicate non-time-of-flight positron-emission tomography system. The bismuth germanate non-time-of-flight positron-emission tomography imaging in a 64 years patient of NHL showing better lesion (spleen) contrast at 2/14 (c) iteration

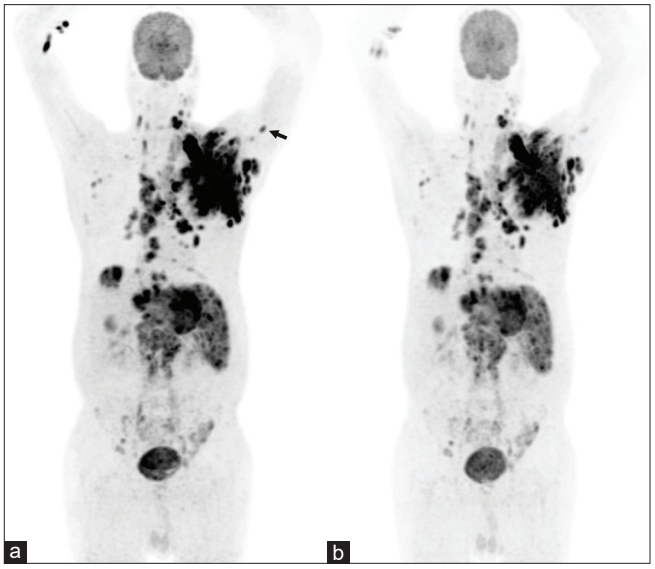

Figure 5: [^{18}F]-fludeoxyglucose positron-emission tomography MIP images reconstructed in time-of-flight (a) and nontime-of-flight mode (b) of a 62-year-old male patient diagnosed with lymphoma showing nearly identical lesions on both the positron-emission tomography systems. A subcentimetric axillary lymph node (<10.0-mm) seen (arrow) more distinctly on lutetium–yttrium oxyorthosilicate time-of-flight system (a) compared to nontime-of-flight counterpart (b)

and Karp, 2009.[20] They reported two times higher image contrast using TOF PET as compared to non-TOF PET. It has also been reported that the TOF model had higher SNR for low-contrast lesions[14] and TOF images allowed better detection of small lesions than the non-TOF images.[21]

To achieve the best performance of these reconstruction parameters, including better image quality and more accurate quantification, it was crucial to optimize reconstruction parameters. Further, the visual image analysis of six patients demonstrated that the best quality PET/CT images were achieved at 2nd and 3rd iterations in TOF and non-TOF systems [Figure 4a-c]. The head-to-head quantitative lesions' analysis revealed that the mean SNR ratio (13.28 ± 6.50) was significantly higher in TOF as compared to the corresponding value (11.76 ± 6.50) in non-TOF system. The TOF model has been known to reduce the BV, thereby improving the image contrast and the detection of subcentimetric lesions/hot spheres.[22]

It was found that after achieving the highest SNR at a given iteration, the value decreased with the increase in the iteration number. SNR and CRC/BV ratios were found to be highest at iteration 2 in TOF and at 3 in non-TOF system. TOF reconstruction converged faster and resulted

Table 4: The signal-to-noise ratio values of the smallest identifiable lesion for lutetium-yttrium oxyorthosilicate time-of-flight and lutetium-yttrium oxyorthosilicate non-time-of-flight systems in six patients using 2/12 and 3/12 iteration/subset reconstruction algorithms

Patient number	SNR (TOF) 2/12	SNR (non-TOF) 3/12
1	15.170	13.607
2	19.901	18.185
3	3.192	0.538
4	7.924	7.997
5	18.928	16.34
6	14.251	13.882
Mean±SD	13.228±6.49	11.758±6.48

SNR: Signal-to-noise ratio, TOF: Time of flight, SD: Standard deviation

Table 5: The signal-to-noise ratio values of the smallest identifiable lesion for bismuth germanate non-time-of-flight system in 10 patients in using 2/14 and 3/14 subset/iteration reconstruction algorithms

Patient number	SNR value for 2/14	SNR value for 3/14
1	0.676	0.9302
2	9.244	9.181
3	15.79	9.966
4	5.50	4.141
5	27.35	17.841
6	51.30	46.675
7	11.37	7.657
8	14.51	13.331
9	18.67	12.495
10	44.98	25.506
Mean±SD	19.93±16.60	14.70±13.16

SNR: Signal-to-noise ratio, SD: Standard deviation

in lower image noise. After too many iterations, when the signal contrast has already converged, the SNR decreases as the image noise increases.[6,13,16] It has been reported that the noise in the PET data had a large impact on the reconstruction process.[21,23] In iterative reconstruction, more noise in the data (from non-TOF PET) obstructs the convergence and therefore causes a reduction in the image contrast, specifically for the small lesions.

An appropriate trade-off between the image contrast and noise is required to obtain the optimum image quality. Furthermore, an iteration number or halting criterion for an iterative algorithm is unpredictable as the same depends on the image noise level. The iteration number, maximizing the SNR for the smallest lesions, differed between TOF and non-TOF reconstructions for the 3D-OSEM algorithm. It was reported that the maximum SNR was observed for 10-mm hot sphere using non-TOF reconstruction at iteration 4, whereas it was observed at iteration 2 in a TOF-based system/reconstruction.[13] Similarly, it was observed that the maximum SNR for 10-mm hot sphere in non-TOF system was found at iteration 3 and at iteration- 2 for TOF system.[24] These studies suggest that there could be small system-to-system variations in reconstruction algorithms which are needed to be established precisely in a given setting. Thus, in the present study, we observed that 2nd and 3rd iterations in LYSO TOF and BGO non-TOF BGO reconstructions provided the best-quality images visually as well as quantitatively. These settings also provided a maximum SNR ratio for the reconstruction of the clinical PET imaging data and this ratio was significantly higher in TOF as compared to non-TOF system.

The performance of either TOF or non-TOF may vary as a function of the patient's physical dimensions, tracer uptake variation, and activity distribution, and hence, a single phantom study may not simulate all clinical imaging conditions. In obese patients of non-Hodgkin lymphoma, the additional lesions were detected more clearly on TOF than on non-TOF images and also showed higher contrast and tracer uptake.[16] According to the NEMA procedural guidelines, the NU 2-2001 IQ body phantom involving both hot and cold lesions simulates images those obtained in a total body imaging study.[25] As observed in the present study, the NEMA IQ phantom image findings have direct translational relevance to the whole-body PET images in patients in terms of the image quality in TOF *versus* non-TOF reconstruction methods and the type of PET scanner. Recently, a digital clinical PET imaging showed 37.0%–44.0% increment in SNR for lesions detected on this imaging in comparison to the SNR seen on analog TOF PET system.[26] Therefore, as a part of the standardization and harmonization and as a good clinical practice, the evaluated PET NEMA phantom factors should be validated for clinical PET data in a given setting.

Conclusion

The use of NEMA IQ phantom demonstrated that the TOF reconstruction converged faster than the non-TOF and provided better SNR and image contrast both for the phantom and patients' PET images. Thus, at the time of installation of new PET scanner/reconstruction software for PET image quantification, the phantom-based standardization of the reconstruction algorithms and validation of the same in a clinical scenario is highly imperative.

Financial support and sponsorship

Nil.

Conflicts of interest

There are no conflicts of interest.

References

1. Coleman RE. PET in lung cancer. J Nucl Med 1999;40:814-20.
2. Delbeke D. Oncological applications of FDG PET imaging: Brain tumors, colorectal cancer, lymphoma and melanoma.

J Nucl Med 1999;40:591-603.
3. Gambhir SS, Czernin J, Schwimmer J, Silverman DH, Coleman RE, Phelps ME. A tabulated summary of the FDG PET literature. J Nucl Med 2001;42:1S-93S.
4. Roop MJ, Singh B, Singh H, Watts A, Kohli PS, Mittal BR, *et al.* Incremental value of Cocktail 18F-FDG and 18F-NaF PET/CT Over 18F-FDG PET/CT alone for characterization of skeletal metastases in breast cancer. Clin Nucl Med 2017;42:335-40.
5. Singh B, Ezziddin S, Palmedo H, Reinhardt M, Strunk H, Tüting T, *et al.* Preoperative 18F-FDG-PET/CT imaging and sentinel node biopsy in the detection of regional lymph node metastases in malignant melanoma. Melanoma Res 2008;18:346-52.
6. Surti S, Karp JS, Popescu LM, Daube-Witherspoon ME, Werner M. Investigation of time-of-flight benefit for fully 3-D PET. IEEE Trans Med Imaging 2006;25:529-38.
7. Tong S, Alessio AM, Kinahan PE. Noise and signal properties in PSF-based fully 3D PET image reconstruction: An experimental evaluation. Phys Med Biol 2010;55:1453-73.
8. Allemand R, Gresset C, Vacher J. Potential advantages of a cesium fluoride scintillator for a time-of-flight positron camera. J Nucl Med 1980;21:153-5.
9. Anger HO. Survey of radioisotope cameras. ISA Trans 1996;5:311-34.
10. Daghighian F, Shenderov P, Pentlow KS, Graham MC, Eshaghian B, Melcher CL, *et al*. Evaluation of cerium doped lutetium oxyorthosilicate (LSO) scintillation crystals for PET. IEEE Trans Nucl Sci 1993;40:1045-7.
11. Melcher CL, Schweitzer JS. Cerium-doped lutetium oxyorthosilicate: A fast, efficient new scintillator. IEEE Trans Nucl Sci 1992;39:502-5.
12. Moses WW, Derenzo SE. Prospects for time-of-flight PET using LSO scintillator. IEEE Trans Nucl Sci 1999;46:474-8.
13. Lois C, Jakoby BW, Long MJ, Hubner KF, Barker DW, Casey ME, *et al.* An assessment of the impact of incorporating time-of-flight information into clinical PET/CT imaging. J Nucl Med 2010;51:237-45.
14. El Fakhri G, Surti S, Trott CM, Scheuermann J, Karp JS. Improvement in lesion detection with whole-body oncologic time-of-flight PET. J Nucl Med 2011;52:347-53.
15. Kadrmas DJ, Casey ME, Conti M, Jakoby BW, Lois C, Townsend DW. Impact of time-of-flight on PET tumor detection. J Nucl Med 2009;50:1315-23.
16. Karp JS, Surti S, Daube-Witherspoon ME, Muehllehner G. Benefit of time-of-flight in PET: Experimental and clinical results. J Nucl Med 2008;49:462-70.
17. Shekari M, Ghafarian P, Ahangari S, Ay M. Quantification of the impact of TOF and PSF on PET images using the noise-matching concept: Clinical and phantom study. Nucl Sci Tech 2017;28:1-8. [Doi: 10.1007/s41365-017-0308-6].
18. Moses WW. Recent advances and future advances in time-of-flight PET. Nucl Instrum Methods Phys Res A 2007;580:919-24.
19. Fukukita H, Suzuki K, Matsumoto K, Terauchi T, Daisaki H, Ikari Y, *et al.* Japanese guideline for the oncology FDG-PET/CT data acquisition protocol: Synopsis of Version 2.0. Ann Nucl Med 2014;28:693-705.
20. Surti S, Karp JS. Experimental evaluation of a simple lesion detection task with time-of-flight PET. Phys Med Biol 2009;54:373-84.
21. Conti M. Focus on time-of-flight PET: The benefits of improved time resolution. Eur J Nucl Med Mol Imaging 2011;38:1147-57.
22. Hashimoto N, Morita K, Tsutsui Y, Himuro K, Baba S, Sasaki M. Time-of-flight information improved the detectability of subcentimeter spheres using a clinical PET/CT scanner. J Nucl Med Technol 2018;46:268-73.
23. Conti M, Townsend D, Casey M, Lois C, Jakoby B, Long M, *et al*. Assessment of the clinical potential of a time-of-flight PET/CT scanner with less than 600ps timing resolution. J Nucl Med 2008;49:411P.
24. Akamatsu G, Ishikawa K, Mitsumoto K, Taniguchi T, Ohya N, Baba S, *et al.* Improvement in PET/CT image quality with a combination of point-spread function and time-of-flight in relation to reconstruction parameters. J Nucl Med 2012;53:1716-22.
25. Daube-Witherspoon ME, Karp JS, Casey ME, DiFilippo FP, Hines H, Muehllehner G, *et al.* PET performance measurements using the NEMA NU 2-2001 standard. J Nucl Med 2002;43:1398-409.
26. Salvadori J, Odille F, Verger A, Olivier P, Karcher G, Marie PY, *et al.* Head-to-head comparison between digital and analog PET of human and phantom images when optimized for maximizing the signal-to-noise ratio from small lesions. EJNMMI Phys 2020;7:11.